Published in final edited form as:

Structure. 2020 January 07; 28(1): 105–110.e3. doi:10.1016/j.str.2019.10.014.

Molecular basis for the PZP domain of BRPF1 association with chromatin

Brianna J. Klein[1,4], **Khan L. Cox**[2,4], **Suk Min Jang**[3], **Jacques Côté**[3], **Michael G. Poirier**[2,*], **Tatiana G. Kutateladze**[1,5,*]

[1]Department of Pharmacology, University of Colorado School of Medicine, Aurora, CO 80045, USA

[2]Department of Physics, Ohio State University, Columbus, Ohio 43210, USA

[3]Laval University Cancer Research Center, CHU de Québec-UL Research Center-Oncology Division, Quebec City, Québec G1R 3S3, Canada

[4]Equal contribution

[5]Lead contact

SUMMARY

The assembly of human histone acetyltransferase MOZ/MORF complexes relies on the scaffolding bromodomain plant homeodomain (PHD) finger 1 (BRPF1) subunit. The PHD-zinc-knuckle-PHD module of BRPF1 ($BRPF1_{PZP}$) has been shown to associate with histone H3 tail and DNA, however the molecular mechanism underlying recognition of H3 and the relationship between the histone and DNA binding activities remain unclear. In this study, we report the crystal structure of $BRPF1_{PZP}$ bound to H3 tail and characterize the role of the bipartite interaction in the engagement of $BRPF1_{PZP}$ with nucleosome core particle (NCP). We find that although both interactions of $BRPF1_{PZP}$ with H3 tail and DNA are required for tight binding to NCP and for acetyltransferase function of the BRPF1-MORF-ING5-MEAF6 complex, binding to extra-nucleosomal DNA dominates. Our findings suggest that functionally active $BRPF1_{PZP}$ might be important in stabilization of the MOZ/MORF complexes at chromatin with accessible DNA.

Graphical Abstract

*Correspondence: tatiana.kutateladze@cuanschutz.edu or poirier.18@osu.edu.

AUTHOR CONTRIBUTIONS

B.J.K., K.L.C. and S.M.J. performed experiments and together with J.C., M.G.P. and T.G.K. analyzed the data. B.J.K. and T.G.K. wrote the manuscript with input from all authors.

DECLARATION OF INTEREST

The authors declare no competing interests.

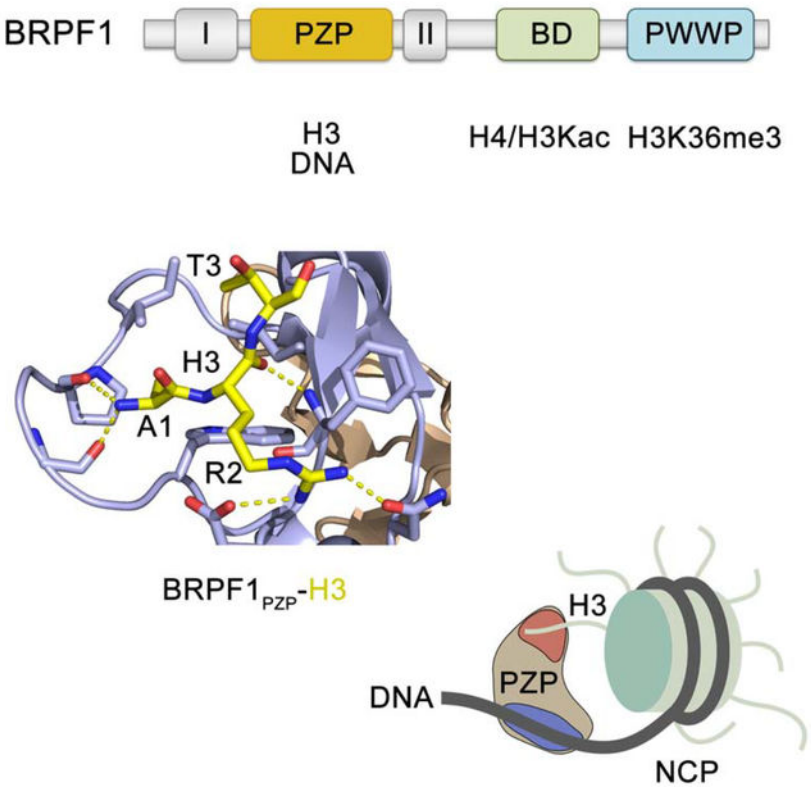

eTOC Blurb

The BRPF1 subunit of human histone acetyltransferase MOZ/MORF complexes is essential for catalytic activity and assembly of these complexes at chromatin. Klein et al. describe the role of bipartite contacts of the PZP domain of BRPF1 with histone and DNA in the engagement with nucleosome and HAT activity of the MORF complex.

Keywords

BRPF1; MORF; MOZ; histone; chromatin; DNA; PZP

INTRODUCTION

Bromodomain and PHD finger containing protein 1 (BRPF1) is a core subunit of the native monocytic leukemic zinc-finger (MOZ) and MOZ related factor (MORF) acetyltransferase complexes that acetylate histones, particularly lysine 23 of histone H3 (H3K23), and mediate transcriptional programs (Huang et al., 2016; Klein and Jang, 2019; Yang, 2015). Genetic studies identified BRPF1 as being essential in the development of brain, axial skeleton and the haematopoietic system, and a large number of mutations and truncations in human BRPF1 have been linked to intellectual disability, congenital abnormalities and leukemias (Demeulenaere et al., 2019; Hibiya et al., 2009; Laue et al., 2008; Mattioli et al., 2017; Mishima et al., 2011; Pode-Shakked et al., 2019; Yan et al., 2017; You et al., 2015a; You et al., 2015b; You et al., 2016). In the complexes, BRPF1 functions as an adaptor

protein which interacts with all other subunits, including the catalytic MOZ/MORF subunit, inhibitor of growth 5 (ING5) and MYST/Esa1-associated factor 6 (MEAF6), and therefore is required for the tetrameric assembly, catalytic activity and substrate specificity of these complexes (Klein et al., 2014a; Yang, 2015).

BRPF1 is a large multimodular protein containing the MOZ/MORF-binding domain (I), a short motif implicated in the interaction with ING5 and MEAF6 (II) (Lalonde et al., 2013a; Ullah et al., 2008), and three histone-binding modules, also known as epigenetic readers characterized by different specificities toward posttranslational modifications in histone proteins (Fig. 1a). The BRPF1 bromodomain (BD) associates with various mono- and poly-acetyllysine-containing sequences in histones H4 and H3 (H4/H3Kac), whereas the PWWP domain recognizes trimethylated K36 of histone H3 (H3K36me3) (Laue et al., 2008; Poplawski et al., 2013; Vezzoli et al.). The central region of BRPF1 harbors two PHD fingers closely linked through a single zinc knuckle, termed the PZP (PHD-zinc-knuckle-PHD) domain ($BRPF1_{PZP}$). Recent biochemical studies have shown that $BRPF1_{PZP}$ binds to unmodified histone H3 tail and is also capable of associating with DNA (Klein et al., 2016). The atomic-resolution structures of the BD and PWWP domains of BRPF1 in complex with their histone ligands provide information that is vital to our understanding of how BRPF1 and the MOZ/MORF complexes localize to genomic regions enriched in H4/H3Kac and H3K36me3 (Laue et al., 2008; Poplawski et al., 2013; Vezzoli et al.). The structures have also been instrumental in the development of numerous small molecule inhibitors for BD of BRPF1, which emerged as one of the promising therapeutic targets in leukemias (Bamborough et al., 2016; Igoe et al., 2017; Zhu and Caflisch, 2016; Zhu et al., 2018), however the structural basis underlying recognition of H3 by $BRPF1_{PZP}$ and the relationship between its histone- and DNA-binding functions remain not well characterized.

Here, we report the molecular mechanism by which $BRPF1_{PZP}$ targets histone H3 tail and DNA and assess contributions of the two binding events to the association of $BRPF1_{PZP}$ with the nucleosome core particle (NCP). We find that while both interactions of $BRPF1_{PZP}$ with H3 tail and DNA are required for tight binding to NCP and for acetyltransferase function of the BRPF1-MORF-ING5-MEAF6 complex, the interaction with extra-nucleosomal DNA predominates.

RESULTS AND DISCUSSION

To determine the molecular basis for the histone H3 recognition by $BRPF1_{PZP}$, we generated a chimeric construct that contains residues 1–12 of H3 fused to residues 271–454 of BRPF1 through a short GSGSS linker. The $^{1}H,^{15}N$ heteronuclear single quantum coherence (HSQC) spectrum of the uniformly ^{15}N-labeled fused H3-PZP construct overlaid well with the spectrum of isolated $BRPF1_{PZP}$ collected in the presence of a five-fold excess of the H3 (residues 1–12) peptide, confirming that the linked and unlinked complexes adopt similar structures in solution (Fig. S1). The fusion protein was crystallized, and the structure of the H3-bound $BRPF1_{PZP}$ was determined to a 2.2 Å resolution (Fig. 1b and Table 1). The structure shows a saddle-like globular fold comprised of five zinc-binding clusters. The Ala1-Thr3 fragment of H3 tail is bound in a shallow groove of the first PHD finger (PHD1) of $BRPF1_{PZP}$. The N-terminal amino group of Ala1 of H3 is restrained by two hydrogen

bonds with the backbone carbonyl groups of P311 and G313 of the protein, whereas the methyl group of Ala1 fits in a hydrophobic cavity formed by L291, I310 and W315 (Fig. 1b, c). The guanidino moiety of Arg2 is constrained via two hydrogen bonds, one to the side chain carboxyl oxygen of D294 and another to the side chain amide oxygen of N297. The backbone amide nitrogen of F292 donates a hydrogen bond to the backbone carbonyl oxygen of Arg2, and the methyl group of Thr3 occupies the same hydrophobic cavity as the methyl group of Ala1 of H3.

Recent studies of AF10, a co-factor of the H3K79-specific methyltransferase DOT1L, show that the PZP domain of AF10 recognizes a middle part of the histone H3 tail, specifically residues Ala21-Lys27 of H3 (Chen et al., 2015). To test whether this binding is conserved in BRPF1, we carried out $^{1}H,^{15}N$ HSQC titration experiments using ^{15}N-labeled $BRPF1_{PZP}$. As expected, the H3 peptide (residues 1–12 of H3) induced large chemical shift perturbations (CSPs) in the $BRPF1_{PZP}$ spectrum, indicating binding, however no CSPs were observed upon titration of the H3 peptide (residues 15–34 of H3), implying that $BRPF1_{PZP}$ does not bind to the middle part of H3 (Fig. 1d). Furthermore, the long H3 peptide (residues 1–31 of H3) caused CSPs in $BRPF1_{PZP}$ almost identical to CSPs caused by the short H3 peptide (residues 1–12), supporting the finding that $BRPF1_{PZP}$ recognizes the far N-terminal but not middle region of H3 tail (Fig. S2).

In addition to recognizing H3, $BRPF1_{PZP}$ was also shown to bind DNA, however the relationship between these functions is not well understood. Electrostatic surface potential of the $BRPF1_{PZP}$:H3 complex reveals that the positively charged residues of PZP involved in DNA binding, particularly K383, K390 and R392, are clustered in the second PHD finger (PHD2) and a zinc knuckle, whereas the negatively charged residues in the first PHD finger (PHD1) form the binding site for H3 (Fig. 2a). Such separation of the binding sites suggests that the two interactions are likely independent of each other. We generated NCP using a 207 bp DNA (NCP_{207}) in which 147 bp 601 Widom DNA is flanked by 30 bp linker DNA on either side and internally labeled with fluorescein 27 bp in from the 5' end and tested binding of $BRPF1_{PZP}$ to NCP_{207} by electrophoretic mobility shift assay (EMSA) and fluorescence polarization. Both wild type (WT) $BRPF1_{PZP}$ and mutants impaired in either H3 binding or DNA binding, including D294K that lost its ability to interact with H3 peptide (Fig. 2b) and K383E/K390E/R392E (KKR) mutant incapable of binding to DNA (Klein et al., 2016), were assayed. NCP_{207} was incubated with increasing amounts of $BRPF1_{PZP}$, and the reaction mixtures were resolved on a 5% native polyacrylamide gel (Fig. 2c). A gradual increase in amount of added WT $BRPF1_{PZP}$ resulted in a shift of the NCP_{207} band, indicative of formation of the $BRPF1_{PZP}$:NCP_{207} complex, however this shift was delayed when $BRPF1_{PZP}$ D294K mutant was used, implying that interaction with H3 is essential for high affinity binding. In contrast, no stable complex with NCP_{207} was formed by $BRPF1_{PZP}$ KKR mutant, indicating that binding to DNA is required for the association with NCP_{207}. These results were substantiated by measuring $S_{1/2}$ in fluorescence anisotropy assays. Titration of WT $BRPF1_{PZP}$ against NCP_{207} yielded a $S_{1/2}$ of 50 μM for the $BRPF1_{PZP}$:NCP_{207} complex formation (Fig. 3a). Binding of the $BRPF1_{PZP}$ D294K mutant to NCP_{207} was two-fold weaker ($S_{1/2}$ = 100 μM), and binding of the $BRPF1_{PZP}$ KKR mutant was undetectable (Fig. 3b, c). The association of WT $BRPF1_{PZP}$ with the nucleosome containing a 147 bp 601 Widom DNA sequence (NCP_{147}) was also

undetectable, confirming that $BRPF1_{PZP}$ prefers extra-nucleosomal DNA (Fig. 3d, e). This preference for the linker DNA might have a significant implication and suggests that functional $BRPF1_{PZP}$ could stabilize the MORF complexes at chromatin regions with accessible DNA, such as euchromatin.

To assess contribution of binding to H3 and DNA by $BRPF1_{PZP}$ to catalytic function of the MORF complex, we produced the MORF complexes by co-transfecting full length HA-BRPF1 with FLAG-$MORF_{N1–716}$, FLAG-ING5 and FLAG-MEAF6 in 293T cells and purified the complexes by immunoprecipitation. The HAT activity of the MORF complexes, containing HA-BRPF1, WT or D294A and $BRPF1_{PZP\Delta}$359–450 (aa 359–450, including K383, K390 and R392 of BRPF1 are deleted) mutants, were measured on human free histones and short oligonucleosomes. The MORF complex containing WT BRPF1 subunit showed a strong HAT activity (Figs. 3f and S3). This activity was decreased three-fold for the BRPF1 D294A mutant defective in H3 binding and five-fold for the $BRPF1_{PZP\Delta}$359–450 mutant defective in DNA binding. Together, these data support the notion that concurrent binding of $BRPF1_{PZP}$ to H3 and DNA is required for proper enzymatic activity of the BRPF1-MORF complex with the latter contributing to a greater degree (Fig. 3e).

$BRPF1_{PZP}$ has expanded a subset of epigenetic readers capable of binding histones and DNA. The dual engagement increases affinity of these readers in the context of chromatin owing to the avidity effect, but relative contribution of the contacts with histones and DNA vary among the readers. For example, interaction of the PWWP domain of LEDGF/PSIP1 with DNA enhances a markedly weak (mM-range) binding of this reader to histone H3K36me3 four orders of magnitude (Eidahl et al., 2013; van Nuland et al., 2013), whereas a relatively weak DNA binding of Tudor, YEATS and bromodomain augments association with NCPs by a few fold (Gibson et al., 2017; Miller et al., 2016; Musselman et al., 2013). In this study, we show that engagement of $BRPF1_{PZP}$ with histone H3 tail and DNA, especially extra-nucleosomal DNA, is required for tight binding to and acetylation of NCP, with the DNA binding activity being more essential. These *in vitro* data are in agreement with previously reported findings that while the HAT activity of the MOZ complex requires both $BRPF1_{PZP}$ functions, the DNA binding rather than histone binding is critical for the association of the complex with chromatin *in vivo* (Klein et al., 2016; Lalonde et al., 2013b). The lesser degree contribution of histone binding could be due to a competitive interaction of the histone tail with DNA and therefore the tail inaccessibility. The intra-nucleosomal histone H3 tail-DNA contacts have been shown to reduce the accessibility of unmodified H3 tails compared to free H3 peptides by up to a factor of ~10 in physiologically relevant conditions (Gatchalian et al., 2017), but strength of these contacts can be modulated by posttranslational modifications (PTMs) in histones (Tencer et al., 2017). It will be interesting in future studies to explore the effect of PTMs, particularly acetylation of distal lysine residues in H3 tail, on bipartite association of $BRPF1_{PZP}$ with NCPs.

STAR METHODS

LEAD CONTACT AND MATERIALS AVAILABILITY

Lead Contact, Tatiana Kutateladze (tatiana.kutateladze@cuanschutz.edu).

All reagents generated in this study will be made available on request, but we may require a payment and/or a completed Materials Transfer Agreement if there is potential for commercial application.

EXPERIMENTAL MODEL AND SUBJECT DETAILS

The PZP domain of BRPF1 and the linked H3-PZP construct were expressed in Rosetta-2 (DE3) pLysS grown in minimal media. Expression was induced with 0.5~1 mM IPTG at A_{600}=0.6–0.8 for 18 h at 16°C.

METHOD DETAILS

QUANTIFICATION AND STATISTICAL ANALYSIS—Statistics generated from X-ray crystallography data processing, refinement, and structure validation are displayed in Table 1.

DATA AND SOFTWARE AVAILABILITY

Software: Software used in this this study has been previously published as detailed in the Key Resources Table.

Data Resources: Coordinates and structure factors have been deposited in the Protein Data Bank under ID code 6U04.

MATERIALS AND METHODS

DNA Cloning and Protein Purification

The PZP domain of BRPF1 (aa 271–454) was cloned into a pDEST15 vector with the N-terminal GST tag and TEV cleavage site. The mutant $BRPF1_{PZP}$ (D294K and K383E/K390E/R392E) constructs were generated using the Stratagene QuickChange XL Site Directed Mutagenesis kit. The sequences were confirmed by DNA sequencing. All proteins were expressed in *Escherichia coli* Rosetta-2 (DE3) pLysS cells grown in minimal media supplemented with $^{15}NH_4Cl$ (Sigma) or NH_4Cl (for unlabeled proteins) and 75 M $ZnCl_2$. Protein production was induced with 0.5 – 1.0 mM IPTG for 18 h at 16°C. B acteria were harvested by centrifugation and lysed by sonication in buffer (50 mM Tris-HCl pH 7.5, 500 mM NaCl, 0.05% (v/v) Nonident P 40, 5 mM dithiothreitol (DTT), 50 M $ZnCl_2$, 5 mM $MgCl_2$, and DNase). GST-fusion proteins were purified on glutathione agarose 4B beads (Thermo Fisher Sci) and the GST-tag was cleaved with tobacco etch virus (TEV) protease. Proteins were further purified by size exclusion chromatography (SEC) and concentrated in Millipore concentrators (Millipore).

X-Ray Crystallography

For structural studies the H3-GSGSS-$BRPF1_{PZP}$ construct (aa 1–12 of histone H3, a GSGSS linker, and aa 271–454 of BRPF1) was cloned into a pDEST15 vector with the N-terminal GST tag and TEV cleavage site. The linked protein was produced as above. Following cleavage with TEV protease and further purification by SEC, the linked H3-PZP protein was concentrated to ~ 6 mg/mL in buffer (50 mM Tris-HCl pH 7.5, 150 mM NaCl, 5 mM DTT) for crystallization. Crystals were grown using sitting-drop diffusion method at 18°C by

mixing 600 nL of protein with 600 nL of well solution composed of 0.2 M Lithium sulfate, 0.1 M Tris-HCl pH 8.5, 40% (v/v) PEG400, and 0.01M Praseodymium(III) acetate hydrate. Crystals were cryoprotected with 30% (v/v) glycerol. X-ray diffraction data were collected from a single crystal on the Anschutz Medical Campus X-ray crystallography core facility Rigaku Micromax 007 high-frequency microfocus X-ray generator equipped with a Pilatus 200K 2D area detector. Indexing and scaling were completed using HKL3000 (Minor et al., 2006). The phase solution was solved with Phenix.phaser (Adams et al., 2010) using molecular replacement and the BRPF1 PZP (PDB ID: 5ERC) structure as the model. Model building was carried out with Coot (Emsley et al., 2010), and refinement was performed with Phenix.refine. The final structure was validated with MolProbity (Chen et al., 2010). Crystallographic statistics for the H3-bound $BRPF1_{PZP}$ structure are shown in Table 1.

NMR experiments

Nuclear magnetic resonance (NMR) experiments were performed at 298 K on a Varian INOVA 600 MHz spectrometer equipped with a cryogenic probe. The $^{1}H,^{15}N$ HSQC spectra of 0.1–0.2 mM uniformly ^{15}N-labeled WT or mutant $BRPF1_{PZP}$ in 50 mM Tris-HCl pH 7.5 buffer, supplemented with 150 mM NaCl, 5 mM dithiothreitol (DTT), and 8% D_2O were collected in the presence of increasing amount of H3 (aa 1–12, 15–34, or 1–31) peptides (synthesized by Synpeptide). NMR data were processed and analyzed with NMRPipe and NMRDraw as previously described (Klein et al., 2014b).

Nucleosome assembly

Human H2A, H2B, H3.2, and H4 histone proteins were expressed in *Escherichia coli* BL21 (DE3) pLysS cells, separated from inclusion bodies and purified using size exclusion and ion exchange chromatography, as described previously (Dyer et al., 2004). Histones were then mixed together in 7 M guanidine HCL, 20 mM Tris-HCl pH 7.5, and 10 mM dithiothreitol in appropriate molar ratios and refolded into octamer by slow dialysis into 2 M NaCl, 20 mM Tris-HCl pH 7.5, 1 mM ethylenediaminetetraacetic acid (EDTA) pH 8.0, and 2 mM β-mercaptoethanol. The octamer was purified from tetramer and dimer by SEC. Octamer was then mixed with 75% excess of DNA in 2 M NaCl, 5 mM Tris pH 8.0 and 0.5 mM EDTA, and NCPs were reconstituted from octamer plus DNA by slow desalting dialysis into 5 mM Tris pH 8.0 and 0.5 mM EDTA. Finally, the NCPs were separated from free DNA via sucrose gradient purification. DNAs used for the NCP assembly were 147 bp 601 Widom DNA fluorescein-labeled on the 5’ end (for NCP_{147}), and 207 bp DNA (147 bp 601 DNA flanked with 30 bp linker DNA on either side and internally labeled with fluorescein 27 bp in from the 5’ end) (for NCP_{207}).

Fluorescence polarization

Fluorescence polarization measurements were carried out by mixing increasing amounts of $BRPF1_{PZP}$, WT or mutants, with 5 nM NCP_{207} or NCP_{147} in 75 mM NaCl, 25 mM Tris-HCl pH 7.5, 0.00625% Tween20, and 5 mM dithiothreitol in a 30 μL reaction volume. The samples were loaded into a Corning round bottom polystyrene plate and allowed to incubate at 4°C for 30 min. The polarization measurements were acquired with a Tecan infinite M1000Pro plate reader by exciting at 470 nm and measuring polarized emission at 519 nm with 5 nm excitation and emission bandwidths. The fluorescence polarization was calculated

from the emission polarized parallel and perpendicular to the polarized excitation light as described previously (Tencer et al., 2017). The data were then fit to a non-cooperative binding isotherm to determine $S_{1/2}$. The $S_{1/2}$ values were averaged over three separate experiments with error calculated as the standard deviation between the runs.

Electrophoretic Mobility Shift Assay

EMSAs were performed by mixing increasing amounts of $BRPF1_{PZP}$, WT or mutants, with 5 nM NCP_{207} in 75 mM NaCl, 25 mM Tris-HCl pH 7.5 buffer, supplemented with 0.00625% Tween20, 10% glycerol and 5 mM dithiothreitol in a 12 μL reaction volume. Each sample was incubated at 4°C for 15 min and then loaded onto a 5% native pol yacrylamide gel. Electrophoresis was performed in 0.3x Tris-borate-EDTA (TBE) at 300 V for 90 min. Fluorescein fluorescence images were acquired with a Typhoon Phosphor Imager.

Purification of wt and mutant BRPF1-MORF-ING5-MEAF6 complexes and HAT assays

Plasmids of full length WT HA-BRPF1, HA-BRPF1 D294A mutant or HA-$BRPF1_{PZP\Delta}$359–450 mutant, together with FLAG-$MORF_{N1–716}$, FLAG-ING5 and FLAG-MEAF6 (Klein et al., 2016) were used to transfect 293T cells by the calcium phosphate method. Cells were harvested 70 h post-cotransfection and nuclear extracts were prepared as previously described (Doyon and Cote, 2016). Purification of HA-BRPF1 complexes after co-transfection was performed essentially as previously described (Avvakumov et al., 2012; Lalonde et al., 2013b). Briefly, anti-HA immunoprecipitation/elution using anti-HA agarose beads (Roche ref:118 150 16001) and 3xHA peptides was followed by anti-Flag immunoprecipitation/elution using FLAG M2 agarose beads (Sigma) and 3xFLAG peptides.

Acetyltransferase activity of the purified complexes was measured with 0.125 Ci of ^{3}H labeled Ac-CoA (2.1 Ci/mmol; PerkinElmer Life Sciences). The HAT reactions were performed in a volume of 15 l using 0.5 g of free histones and short oligonucleosomes (purified from HeLa cells) as substrates, in HAT buffer (50 mM Tris-HCl pH 8, 50 mM KCl, 10 mM sodium butyrate, 5% glycerol, 0.1 mM EDTA, 1 mM dithiothreitol for 30 minutes at 30°C. The reactions were then captured on P81 filter paper, the free ^{3}H-labeled Ac-CoA was washed away, and the paper was analyzed using Liquid Scintillation.

Supplementary Material

Refer to Web version on PubMed Central for supplementary material.

ACKNOWLEDGEMENTS

We thank JaeWoo Ahn for help with experiments and X.J. Yang for kindly providing cDNA of FLAG-$MORF_{N1-716}$. This work was supported by grants from NIH GM100907 and GM125195 to T.G.K., and GM120582, GM121966 and GM131626 to M.G.P. and from Canadian Institutes of Health Research (CIHR FDN-143314) to J.C. J.C. holds the Canada Research Chair in Chromatin Biology and Molecular Epigenetics.

References

Adams PD, Afonine PV, Bunkoczi G, Chen VB, Davis IW, Echols N, Headd JJ, Hung LW, Kapral GJ, Grosse-Kunstleve RW, et al. (2010). PHENIX: a comprehensive Python-based system for

macromolecular structure solution. Acta crystallographica. Section D, Biological crystallography 66, 213–221. [PubMed: 20124702]

Avvakumov N, Lalonde ME, Saksouk N, Paquet E, Glass KC, Landry AJ, Doyon Y, Cayrou C, Robitaille GA, Richard DE, et al. (2012). Conserved molecular interactions within the HBO1 acetyltransferase complexes regulate cell proliferation. Molecular and cellular biology 32, 689–703. [PubMed: 22144582]

Bamborough P, Barnett HA, Becher I, Bird MJ, Chung CW, Craggs PD, Demont EH, Diallo H, Fallon DJ, Gordon LJ, et al. (2016). GSK6853, a Chemical Probe for Inhibition of the BRPF1 Bromodomain. ACS Med Chem Lett 7, 552–557. [PubMed: 27326325]

Chen S, Yang Z, Wilkinson AW, Deshpande AJ, Sidoli S, Krajewski K, Strahl BD, Garcia BA, Armstrong SA, Patel DJ, and Gozani O (2015). The PZP Domain of AF10 Senses Unmodified H3K27 to Regulate DOT1L-Mediated Methylation of H3K79. Molecular cell 60, 319–327. [PubMed: 26439302]

Chen VB, Arendall WB 3rd, Headd JJ, Keedy DA, Immormino RM, Kapral GJ, Murray LW, Richardson JS, and Richardson DC (2010). MolProbity: all-atom structure validation for macromolecular crystallography. Acta crystallographica. Section D, Biological crystallography 66, 12–21. [PubMed: 20057044]

Demeulenaere S, Beysen D, De Veuster I, Reyniers E, Kooy F, and Meuwissen M (2019). Novel BRPF1 mutation in a boy with intellectual disability, coloboma, facial nerve palsy and hypoplasia of the corpus callosum. Eur J Med Genet 62, 103691. [PubMed: 31176769]

Doyon Y, and Cote J (2016). Preparation and Analysis of Native Chromatin-Modifying Complexes. Methods in enzymology 573, 303–318. [PubMed: 27372759]

Dyer PN, Edayathumangalam RS, White CL, Bao Y, Chakravarthy S, Muthurajan UM, and Luger K (2004). Reconstitution of nucleosome core particles from recombinant histones and DNA. Methods in enzymology 375, 23–44. [PubMed: 14870657]

Eidahl JO, Crowe BL, North JA, McKee CJ, Shkriabai N, Feng L, Plumb M, Graham RL, Gorelick RJ, Hess S, et al. (2013). Structural basis for high-affinity binding of LEDGF PWWP to mononucleosomes. Nucleic acids research 41, 3924–3936. [PubMed: 23396443]

Emsley P, Lohkamp B, Scott WG, and Cowtan K (2010). Features and development of Coot. Acta crystallographica. Section D, Biological crystallography 66, 486–501. [PubMed: 20383002]

Gatchalian J, Wang X, Ikebe J, Cox KL, Tencer AH, Zhang Y, Burge NL, Di L, Gibson MD, Musselman CA, et al. (2017). Accessibility of the histone H3 tail in the nucleosome for binding of paired readers. Nature communications 8, 1489.

Gibson MD, Gatchalian J, Slater A, Kutateladze TG, and Poirier MG (2017). PHF1 Tudor and N-terminal domains synergistically target partially unwrapped nucleosomes to increase DNA accessibility. Nucleic acids research.

Hibiya K, Katsumoto T, Kondo T, Kitabayashi I, and Kudo A (2009). Brpf1, a subunit of the MOZ histone acetyl transferase complex, maintains expression of anterior and posterior Hox genes for proper patterning of craniofacial and caudal skeletons. Developmental biology 329, 176–190. [PubMed: 19254709]

Huang F, Abmayr SM, and Workman JL (2016). Regulation of KAT6 Acetyltransferases and Their Roles in Cell Cycle Progression, Stem Cell Maintenance, and Human Disease. Molecular and cellular biology 36, 1900–1907. [PubMed: 27185879]

Igoe N, Bayle ED, Fedorov O, Tallant C, Savitsky P, Rogers C, Owen DR, Deb G, Somervaille TC, Andrews DM, et al. (2017). Design of a Biased Potent Small Molecule Inhibitor of the Bromodomain and PHD Finger-Containing (BRPF) Proteins Suitable for Cellular and in Vivo Studies. Journal of medicinal chemistry 60, 668–680. [PubMed: 28068087]

Klein BJ, and Jang e.a. (2019). Histone H3K23-specific acetylation by MORF is coupled to H3K14 acylation. Nature communications.

Klein BJ, Lalonde ME, Cote J, Yang XJ, and Kutateladze TG (2014a). Crosstalk between epigenetic readers regulates the MOZ/MORF HAT complexes. Epigenetics 9, 186–193. [PubMed: 24169304]

Klein BJ, Muthurajan UM, Lalonde ME, Gibson MD, Andrews FH, Hepler M, Machida S, Yan K, Kurumizaka H, Poirier MG, et al. (2016). Bivalent interaction of the PZP domain of BRPF1 with

the nucleosome impacts chromatin dynamics and acetylation. Nucleic acids research 44, 472–484. [PubMed: 26626149]

Klein BJ, Piao L, Xi Y, Rincon-Arano H, Rothbart SB, Peng D, Wen H, Larson C, Zhang X, Zheng X, et al. (2014b). The Histone-H3K4-Specific Demethylase KDM5B Binds to Its Substrate and Product through Distinct PHD Fingers. Cell reports 6, 325–335. [PubMed: 24412361]

Lalonde ME, Avvakumov N, Glass CK, Joncas FH, Saksouk N, Holliday M, Paquet E, Yan K, Tong Q, Klein BJ, et al. (2013a). Exchange of associated factors directs a switch in HBO1 acetyltransferase histone tail specificity. Genes Dev in press.

Lalonde ME, Avvakumov N, Glass KC, Joncas FH, Saksouk N, Holliday M, Paquet E, Yan K, Tong Q, Klein BJ, et al. (2013b). Exchange of associated factors directs a switch in HBO1 acetyltransferase histone tail specificity. Genes Dev 27, 2009–2024. [PubMed: 24065767]

Laue K, Daujat S, Crump JG, Plaster N, Roehl HH, Kimmel CB, Schneider R, and Hammerschmidt M (2008). The multidomain protein Brpf1 binds histones and is required for Hox gene expression and segmental identity. Development 135, 1935–1946. [PubMed: 18469222]

Mattioli F, Schaefer E, Magee A, Mark P, Mancini GM, Dieterich K, Von Allmen G, Alders M, Coutton C, van Slegtenhorst M, et al. (2017). Mutations in Histone Acetylase Modifier BRPF1 Cause an Autosomal-Dominant Form of Intellectual Disability with Associated Ptosis. American journal of human genetics 100, 105–116. [PubMed: 27939639]

Miller TC, Simon B, Rybin V, Grotsch H, Curtet S, Khochbin S, Carlomagno T, and Muller CW (2016). A bromodomain-DNA interaction facilitates acetylation-dependent bivalent nucleosome recognition by the BET protein BRDT. Nature communications 7, 13855.

Minor W, Cymborowski M, Otwinowski Z, and Chruszcz M (2006). HKL-3000: the integration of data reduction and structure solution--from diffraction images to an initial model in minutes. Acta crystallographica. Section D, Biological crystallography 62, 859–866. [PubMed: 16855301]

Mishima Y, Miyagi S, Saraya A, Negishi M, Endoh M, Endo TA, Toyoda T, Shinga J, Katsumoto T, Chiba T, et al. (2011). The Hbo1-Brd1/Brpf2 complex is responsible for global acetylation of H3K14 and required for fetal liver erythropoiesis. Blood 118, 2443–2453. [PubMed: 21753189]

Musselman CA, Gibson MD, Hartwick EW, North JA, Gatchalian J, Poirier MG, and Kutateladze TG (2013). Binding of PHF1 Tudor to H3K36me3 enhances nucleosome accessibility. Nature communications 4, 2969.

Pode-Shakked N, Barel O, Pode-Shakked B, Eliyahu A, Singer A, Nayshool O, Kol N, Raas-Rothschild A, Pras E, and Shohat M (2019). BRPF1-associated intellectual disability, ptosis, and facial dysmorphism in a multiplex family. Mol Genet Genomic Med 7, e665. [PubMed: 31020800]

Poplawski A, Hu K, Lee W, Natesan S, Peng D, Carlson S, Shi X, Balaz S, Markley JL, and Glass KC (2013). Molecular Insights into the Recognition of N-Terminal Histone Modifications by the BRPF1 Bromodomain. Journal of molecular biology.

Tencer AH, Cox KL, Di L, Bridgers JB, Lyu J, Wang X, Sims JK, Weaver TM, Allen HF, Zhang Y, et al. (2017). Covalent Modifications of Histone H3K9 Promote Binding of CHD3. Cell reports 21, 455–466. [PubMed: 29020631]

Ullah M, Pelletier N, Xiao L, Zhao SP, Wang K, Degerny C, Tahmasebi S, Cayrou C, Doyon Y, Goh SL, et al. (2008). Molecular architecture of quartet MOZ/MORF histone acetyltransferase complexes. Molecular and cellular biology 28, 6828–6843. [PubMed: 18794358]

van Nuland R, van Schaik FM, Simonis M, van Heesch S, Cuppen E, Boelens R, Timmers HM, and van Ingen H (2013). Nucleosomal DNA binding drives the recognition of H3K36-methylated nucleosomes by the PSIP1-PWWP domain. Epigenetics & chromatin 6, 12. [PubMed: 23656834]

Vezzoli A, Bonadies N, Allen MD, Freund SM, Santiveri CM, Kvinlaug BT, Huntly BJ, Gottgens B, and Bycroft M (2010). Molecular basis of histone H3K36me3 recognition by the PWWP domain of Brpf1. Nature structural & molecular biology 17, 617–619.

Yan K, Rousseau J, Littlejohn RO, Kiss C, Lehman A, Rosenfeld JA, Stumpel CTR, Stegmann APA, Robak L, Scaglia F, et al. (2017). Mutations in the Chromatin Regulator Gene BRPF1 Cause Syndromic Intellectual Disability and Deficient Histone Acetylation. American journal of human genetics 100, 91–104. [PubMed: 27939640]

Yang XJ (2015). MOZ and MORF acetyltransferases: Molecular interaction, animal development and human disease. Biochimica et biophysica acta 1853, 1818–1826. [PubMed: 25920810]

You L, Yan K, Zhou J, Zhao H, Bertos NR, Park M, Wang E, and Yang XJ (2015a). The lysine acetyltransferase activator Brpf1 governs dentate gyrus development through neural stem cells and progenitors. PLoS genetics 11, e1005034. [PubMed: 25757017]

You L, Zou J, Zhao H, Bertos NR, Park M, Wang E, and Yang XJ (2015b). Deficiency of the chromatin regulator BRPF1 causes abnormal brain development. The Journal of biological chemistry 290, 7114–7129. [PubMed: 25568313]

You LY, Li L, Zou JF, Yan KZ, Belle J, Nijnik A, Wang E, and Yang XJ (2016). BRPF1 is essential for development of fetal hematopoietic stem cells. Journal of Clinical Investigation 126, 3247–3262. [PubMed: 27500495]

Zhu J, and Caflisch A (2016). Twenty Crystal Structures of Bromodomain and PHD Finger Containing Protein 1 (BRPF1)/Ligand Complexes Reveal Conserved Binding Motifs and Rare Interactions. Journal of medicinal chemistry 59, 5555–5561. [PubMed: 27167503]

Zhu J, Zhou C, and Caflisch A (2018). Structure-based discovery of selective BRPF1 bromodomain inhibitors. Eur J Med Chem 155, 337–352. [PubMed: 29902720]

HIGLIGHTS

- Tight association of $BRPF1_{PZP}$ with nucleosome requires binding to H3 tail and DNA
- Interaction of $BRPF1_{PZP}$ with DNA contributes to a higher degree
- $BRPF1_{PZP}$ shows preference for extra-nucleosomal DNA

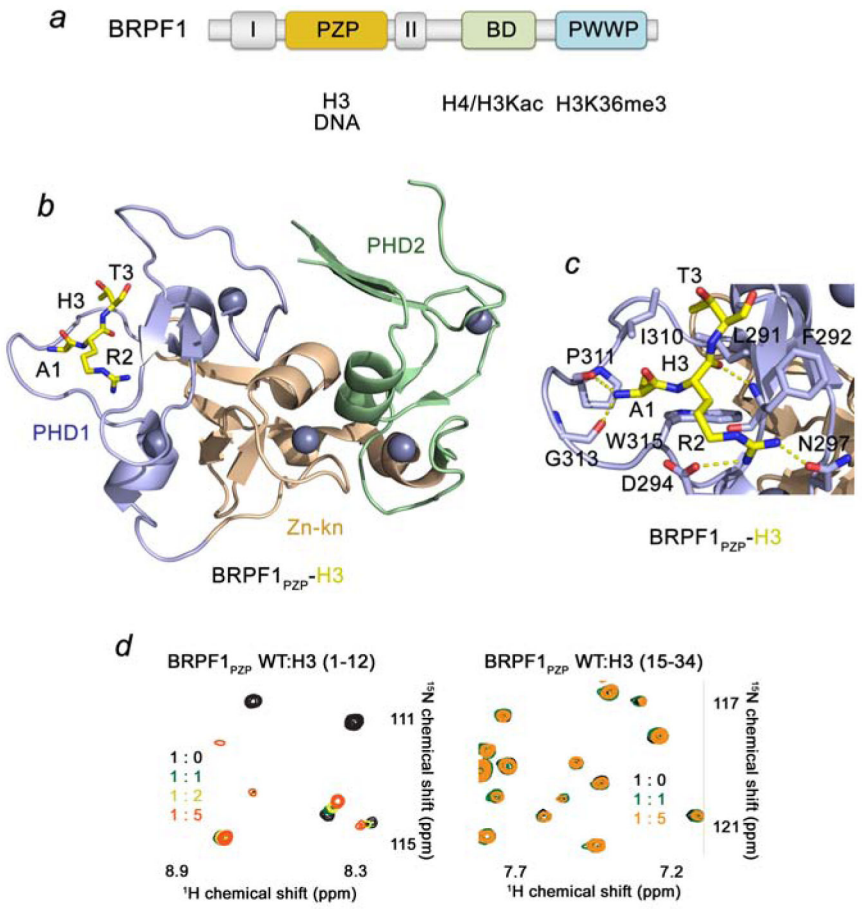

Figure 1. BRPF1$_{PZP}$ recognizes the N-terminal part of H3 tail.

(a) BRPF1 domain architecture. (b) The crystal structure of the H3-bound BRPF1$_{PZP}$ is depicted in a ribbon diagram with PHD1, Zn-kn and PHD2 colored blue, wheat, and green, respectively. The Ala1-Thr3 fragment of the H3 tail is shown as yellow sticks, and the zinc ions are grey spheres. (c) Close up view of the H3 binding pocket. Hydrogen bonds between residues of H3 tail and PHD1 indicated by yellow dash lines. (d) Superimposed $^{1}H,^{15}N$ HSQC spectra of BRPF1$_{PZP}$ collected in the presence of increasing amounts of H3 peptide (residues 1–12 on the left, and residues 15–34 on the right). The spectra are color-coded according to the protein-peptide ratio (inset). See also Figures S1 and S2.

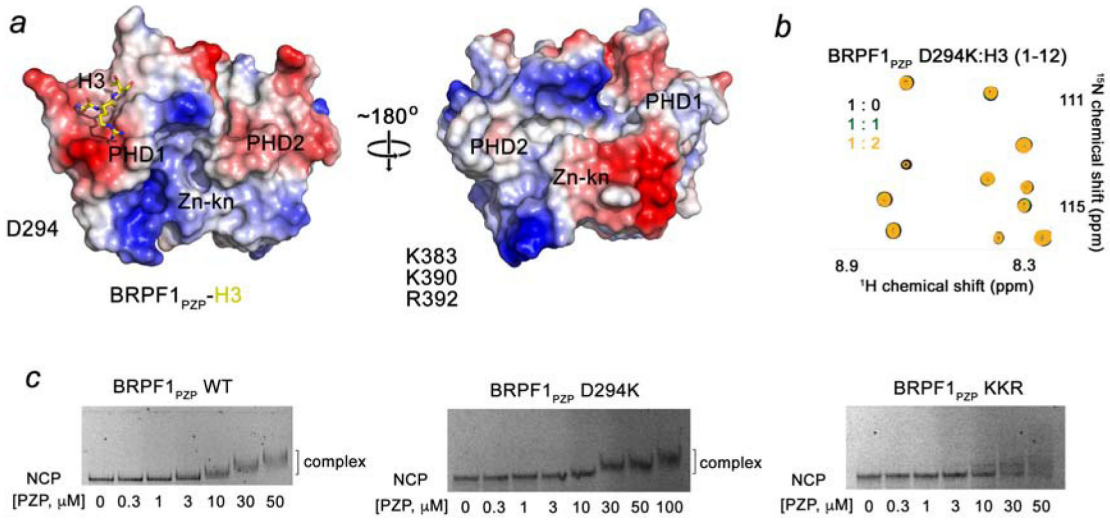

Figure 2. BRPF1$_{PZP}$ binds to nucleosomes in a bivalent manner.

(a) Electrostatic surface potential of BRPF1$_{PZP}$ in the complex with blue and red colors representing positive and negative charges, respectively. The H3 tail is shown in yellow sticks. (b) Superimposed ^{1}H,^{15}N HSQC spectra of BRPF1$_{PZP}$ D294K mutant recorded in the presence of increasing amount of H3 peptide (residues 1–12). The spectra are color-coded according to the protein-peptide ratio (inset). (c) EMSA with NCP$_{207}$ incubated with increasing amounts of the indicated BRPF1$_{PZP}$ proteins. Amount of each protein mixed with 5 nM NCP$_{207}$ is shown below each gel image.

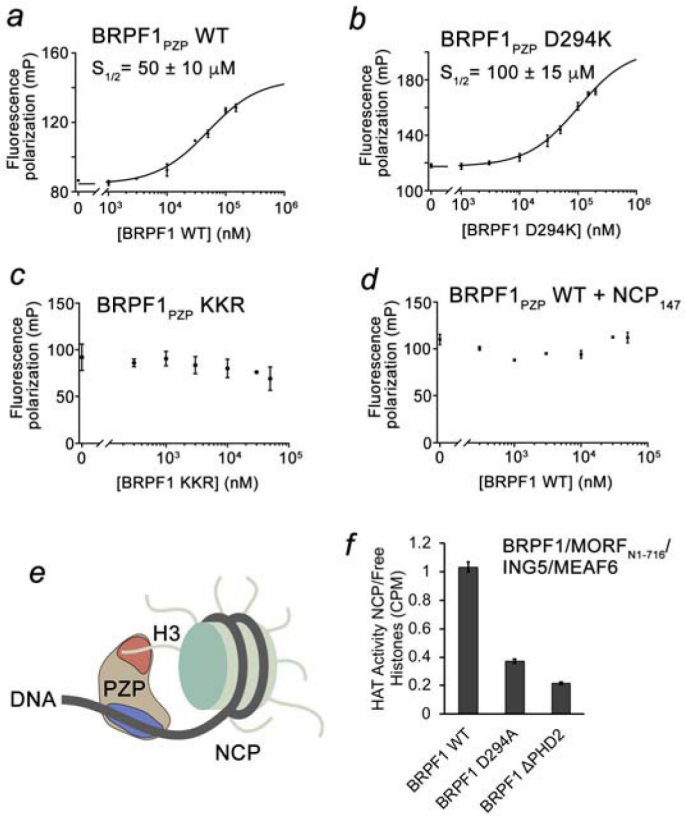

Figure 3. Binding of BRPF1$_{PZP}$ to DNA predominates.

(a-d) Binding curves obtained for the interactions of indicated BRPF1$_{PZP}$ proteins with NCP$_{207}$ (a-c) or NCP$_{147}$ (d) in fluorescence polarization assays. Error bars are SD based on three separate experiments. (e) A model of the bivalent interaction of BRPF1$_{PZP}$ with histone H3 of the nucleosome and extra-nucleosomal DNA. (f) Ratio of HAT activities of the WT and mutant BRPF1-MORF-ING5-MEAF6 complexes on nucleosomes versus free histones. HA-BRPF1, wild type (WT) or mutants (D294A and BRPF1$_{PZP\Delta}$359–450), FLAG-MORF$_{N1–716}$ (aa 1–716 of MORF, containing the catalytic MYST domain), FLAG-ING5 and FLAG-MEAF6 were used to transfect 293T cells. Error bars indicate the range from duplicate samples. Background counts obtained with fractions from mock transfections were subtracted (~150 cpms). See also Figure S3.

Table 1.

Data collection and refinement statics for the H3-BRPF1$_{PZP}$ complex.

	H3-linked BRPF1 PZP
Data collection	
Space group	P 61 2 2
Cell dimensions	
a, *b*, *c* (Å)	72.5, 72.5, 155.3
α, β, γ (°)	90, 90, 120
Resolution (Å)	2.20(2.28–2.20) *
R_{pim}	0.032(0.177)
$I / \sigma I$	25.3(4.4)
Completeness (%)	99.5(100)
Redundancy	20.8(20.7)
Refinement	
Resolution (Å)	22.7–2.2
No. reflections	12773
R_{work} / R_{free}	0.1720/0.2085
No. atoms	1432
BRPF1 PZP	1295
H3	23
Zn	5
PR	1
Water	108
B-factors	38.00
BRPF1 PZP	36.97
H3	80.90
Zn	29.42
PR	64.51
Water	41.45
R.m.s. deviations	
Bond lengths (Å)	0.007
Bond angles (°)	0.978
Ramachandran Plot	
Favored (%)	98.12
Allowed (%)	1.88
Outliers (%)	0

* Values in parentheses are for highest-resolution shell.

KEY RESOURCES TABLE

REAGENT or RESOURCE	SOURCE	IDENTIFIER
Bacterial and Virus Strains		
Escherichia coli Rosetta-2 (DE3) pLysS	Novagen-Thermo Fisher Sci	71-401-3
Escherichia coli BL21 DE3 pLysS	Promega	L1195
Chemicals, Peptides, and Recombinant Proteins		
Dithiothreitol	Gold Biotechnology	27565-41-9
15NH4Cl	Sigma-Aldrich	299251
IPTG	Gold biotechnology	I2481C100
Glutatahione Sepharose 4B beads	Thermo Fisher Sci	16101
H3 peptides (1–12aa, 15–34aa, and 1–31aa)	Synpeptide	N/A
Tobacco etch virus (TEV) protease	**van den Berg et al., 2006**	N/A
Deposited Data		
Protein Data Bank	This study	PDB ID 6U04
Protein Data Bank	Klein et al., 2016	PDB ID 5ERC
Oligonucleotides		
Primer: D294K Forward: aatgtcatcctcttctgtaagatgtgcaacctggccgtg	This study - IDT	N/A
Primer: D294K Reverse: cacggccaggttgcacatcttacagaagaggatgacatt	This study - IDT	N/A
Primer: KKR Forward: caccagctcgctgggaactcacctgctac	This study - IDT	N/A
Primer: KKR Forward: acctgctacatttgcgaacaagagggctcaggggcctgcatccagtgc	This study - IDT	N/A
Primer: KKR Reverse: gtagcaggtgagttcccagcgagctggtg	This study - IDT	N/A
Primer: KKR Reverse: gcactggatgcaggcccctgagccctcttgttcgcaaatgtagcaggt	This study - IDT	N/A
Recombinant DNA		
Plasmid: pDEST15	Thermo Fisher Sci	1180214
Software and Algorithms		
HKL3000	Minor et al., 2006	
Phenix	Adams et al., 2010	N/A
Coot	Emsley et al., 2010	N/A
MOLProbity	Chen et al., 2010	N/A